Technique to Differentiate Between Surface Nanostructuring and Hardening

[1]Pramod Kumar, [2]Mohd. Anas
[1]Department of Mechanical Engineering, Integral University,
[2]Department of Mechanical Engineering, Integral University,

Abstract - The surface nanostructuring along with hardening is a novel process that has been developed to enhance fatigue and wear resistances. The surface nanostructuring and hardening is similar to widely used shot peening in the sense that both processes comprises of repeated impacts of the work-piece surface with spheres. The difference between them lies in the sizes of spheres and the impact velocities used. Such a difference results in dramatic changes in kinetic energies and thus the thicknesses of the work-hardened layer and the nano-grained layer. By a finite element modelling technique a quantitative description of these differences can be seen. The results show that the kinetic energy in the SNH process is typically 180 times larger than that in shot peening, and the deformation layer in the SNH process is about 10 times thicker than that generated in shot peening. Furthermore, the maximum plastic strain and the maximum residual compressive stresses in the SNH-processed work-piece are 100 and 10 times larger than those in the shot-peened work-piece, respectively.

Index Terms - surface nanostructuring, hardening, compressive stresses etc.

I. INTRODUCTION

Severe plastic deformation (SPD) is an important surface nanostructuring process that has recently been developed to produce engineering components with a surface nanocrystalline (nc) layer and a coarse-grained interior. The processes based on SPD are generally referred to as surface mechanical attrition treatment (SMAT) [1,2]. The key feature for these processes is the impact of the work-piece surface by high-velocity balls. The high velocity of balls is typically generated through collision between balls and a vibrating chamber driven by an ultrasonic generator (previously named as ultrasonic shot peening (USSP) [3,4]) or by an electric motor (previously known as high energy shot peening (HESP) [5,6], surface mechanical attrition (SMA), surface mechanical attrition treatment [1,2], or surface nanostructuring and hardening (SNH) [7,8]). The high velocity of balls has also been generated through a high-pressure light-gas gun which accelerates particles to a desired impact velocity, named as the particle impact processing (PIP) [9,10]. These SPD-based processes can result in a nanostructured surface layer up to about 50 μm thick [11], and have been shown to improve the tensile strength [12], microhardness [13], wear resistance [14], and fatigue strength [15] of materials.

The SPD-based processes are almost same to conventionally used shot peening (SP) in the sense that all of these processes shows repeated impacts of the work-piece surface by high-speed balls. However, it is well known that surface nanostructuring has not always been observed in SP. The reason behind such a discrepancy between the SPD-based processes and SP is believed to stem from their large differences in kinetic energies of impinging balls.

Table 1
Typical parameters of balls and shots used in SP and various SMAT processes

Process	diameter of balls or shots (mm)	Impact velocity (m/s)	Kinetic energy of balls or shots (J)
SP [16,17]	0.25–1.0	20–150	9.2×10^{-6}–0.01
USSP [3,4]	0.4–3.0	<2	0.0001–0.02
SMAT [1,2]	2.0–10.0	2–5	<0.2
HESP [5,6]	4.0–8.0	2–3	<0.018
SNH [7,8,15]	4.0–8.0	5–15	0.0063–0.43
PIP [9,10]	4	120	1.88

Table 1 enlists typical values for the ball sizes and speeds used in SPD-based processes and SP reported in literature [1–10,15–17]. Their corresponding kinetic energies are also included for comparison. It can be seen that the difference between the SPD-based processes and SP lies in the sizes of spheres and the impact velocities used. Such a difference results in dramatic changes in kinetic energies. It can be seen that PIP has the highest kinetic energy, followed by SNH and SMAT, and then HESP. SP has the lowest kinetic energy which may overlap with the kinetic energy of USSP, depending on the diameter and velocity of balls and shots used.

Kinetic energy is also dependent of the density of the ball and shot used. It is assumed that WC balls and shots are used in all of these processes.

In a study done by finite element modeling technique a quantitative difference between SNH and SP, and effect of kinetic energies on the surface nanostructuring, the thickness of the work-hardened layer, and the distribution and magnitude of residual compressive stresses. As will be shown in the following sections, the present study confirms that the kinetic energies of balls and shots are indeed critical parameters in determining the degree of surface severe plastic deformation and the mechanical and microstructural features of the work-piece surface. Based on these analyses, it is expected that the SPD-processed work-piece will have better fatigue resistance than the shot-peened work-piece. The details of these analyses are shown below.

1.1 Model used

Fig. 1 shows the single-ball-impact model developed in this study. In this model, a nickel-based HASTELLOY® C-20001 plate with a nominal chemical composition (in weight per-cent) of 23Cr, 16Mo, 1.6Cu, 0.01C, 0.08Si, and balance Ni was assumed to be the work-piece impacted by a WC ball.

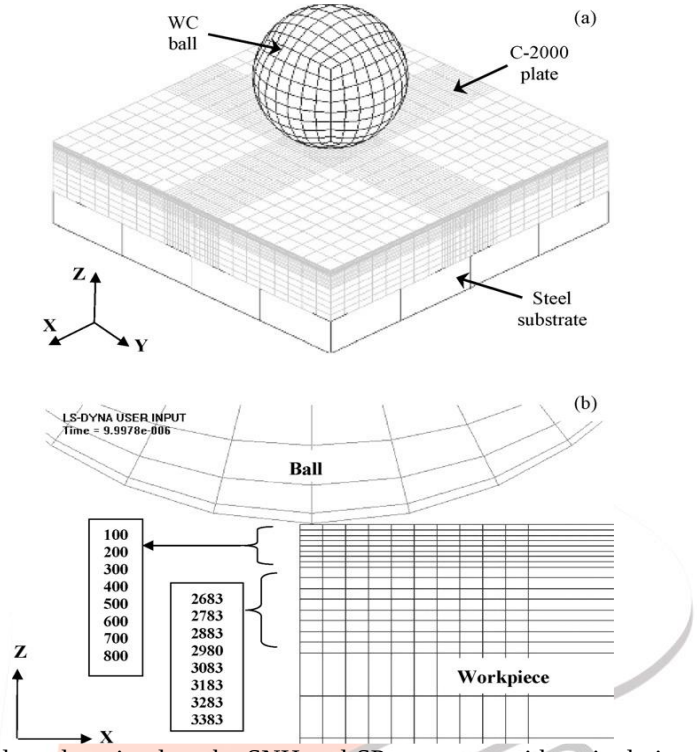

Fig. 1. (a) The finite element model used to simulate the SNH and SP processes with a single impact, and (b) a cross-sectional view of the mesh passing through the center of the plate shown in (a) with element numbers in the first column of the elements indicated.

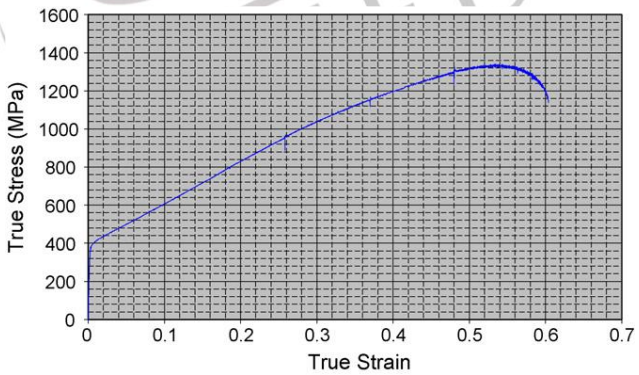

Fig. 2. The experimentally determined true stress–strain curve of the C-2000 conventional alloy

Table 2

Case ID	Ball diameter (mm)	Impact velocity (m/s)	Kinetic energy (J)	Kinetic energy ratio of Case Ito Case II or III
Case I (SNH)	7.86	5	0.0476	1
Case II (SP)	0.3	50	0.000265	180
Case III (SP)[a]	0.3	670	0.0476	1

The C-2000 plate with size 20x20x3.2mm which is backed by a steel substrate to provide a rigid support to the plate. The substrate and ball were modeled as rigid materials, while the C-2000 plate was modeled as an elasto-plastic material. The tensile true stress–strain curve of the C-2000 plate was measured experimentally at room temperature with a constant strain rate of 5 × 10-4 s-1 and shown in Fig. 2. C-2000 plate showed the plastic behavior in the model was based on this measured stress–strain curve, while the elastic properties of the C-2000 plate and WC balls were based on available data in literature[16, 17]. Specifically, the density, Young's modulus and Poisson's ratio of the same plate were 8.5 g/cm^3, 197 GPa, and 0.4, respectively, whereas the corresponding values for WC balls were 14.5 g/cm^3, 600 GPa, and 0.3. The elastic properties of the steel substrate were chosen to be 7.85 g/cm^3 for its density, 200 GPa for the Young's modulus, and 0.3 for the Poisson's ratio.

The effect of temperature rise during impact was neglected in the model because the temperature rise during impact was very small (~43 °C only). This temperature rise was found by assuming adiabatic heating during each impact. As will be shown in Section 3, the maximum effective plastic strain in the work-piece induced upon the first impact is about 0.19. We assume that all this plastic work was converted to heat, then the temperature rise per unit volume was found to be about 43 °C. The effect of strain rate on the material properties was not included in the model either. Pure Ni has a low strain rate sensitivity (<0.008), while Ni alloys may have pronounced strain rate sensitivities (>0.07). Because of the lack of the experimental data for the strain rate sensitivity of the C-2000 alloy, the effect of the strain rate sensitivity was not included in the model. Although such an approximation could result in lower values of the flow stress, but would not change the trend investigated in this study.

During simulation, the nodes at the four edges of the plate were fixed in all directions, while all other nodes were free to move in *x, y,* and *z* directions. Such a boundary condition approximated the particular situation of the experiment in which the plate was fixed at the edges against the substrate with the top surface being impacted by WC balls. In order to ensure the calculation accuracy, the mesh in the top center of the plate being impacted by the ball was much finer than that in the other regions. The dimensions of the element in the impacted region were 0.333mm × 0.333mm × 0.15 mm.

Table 2 describes the three cases of ball-impacting and their input data for the ball sizes and velocities that have been investigated in this study. Cases I and II are typical SNH and SP processes, respectively. Case III is a hypothetical high-speed shot peening process having the identical kinetic energy as Case I. Comparisons between Cases I and III can provide the insight into the effect of the ball size when the kinetic energy is kept constant. Single-ball-impact events were numerically modeled for all three cases, whereas multiple ball impacts (~770 impacts) were further analyzed for Case I. In simulating the multiple impact events, a C-2000 disc, rather than a square plate, with a diameter of 19 mm and thickness 1.6mm in was analyzed. Furthermore, the impact locations in the multiple impact model were completely random and generated by the randomize function of Rnd() in Microsoft Visual Basic language. It was assumed that impact events were independent from one another.

The numerical simulation of both single and multiple impacts was carried out using a finite element code, LS-DYNA, which is a 3D finite element code designed for transient dynamic analysis of nonlinear problems, such as elastic–plastic, large deformation, dynamic contact, etc. It is developed by Livermore Software Technology Corporation (LSTC) [18]. The explicit dynamic solver is used in LS-DYNA to handle impact loading. Thus, no convergence control is needed in LS-DYNA because of the use of explicit time integration in the code which requires no iteration of nonlinear systems. 3D solids elements with flexible body contact, flexible body to rigid body contact, and rigid body to rigid body contact capabilities were used in this study to simulate impact events.

II. RESULTS AND DISCUSSION

2.1 SNH process with Single impacts

Fig. 3 shows the *x*- and *z*-stresses in the C-2000 plate right at the contact point with the ball as a function of the impacting time. At slightly larger than 1 × 10^{-5} s, the WC ball contacts the plate, which immediately (in less than 1 × 10^{-5} s) generates a huge compressive *x*-stress (in the plane of the work-piece) as well as a huge compressive *z*-stress (in the direction of the plate thickness). The magnitudes of compressive stresses are substantially higher than the tensile yield strength of the C-2000 plate (400 MPa), indicating the presence of large hydrostatic compressive force induced by the impact of the high-speed WC ball. Soon after the maximum compressive stresses are reached at ~2 × 10^{-5} s, both *x*- and *z*-stresses are reduced. Such a reduction in the compressive stresses is not due to a decrease in the contact force in the *z*-direction, but caused by the increase in the contact area between the ball and plate. This conclusion can be confirmed by examining Fig. 4, which shows that the contact force in the *z*-direction continues to increase during the period in which the *x*- and *z*-stresses exhibit a decrease.

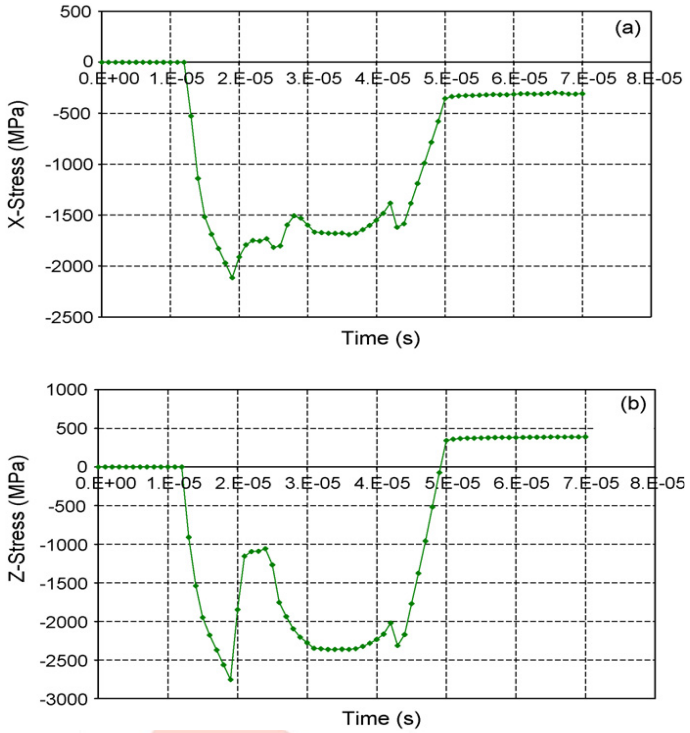

Fig. 3. (a) The x-stress and (b) the z-stress in the work-piece right at the contact point with the impacting ball (i.e., element 100 in Fig. 1b) as a function of the impacting time for Case I in Table 2.

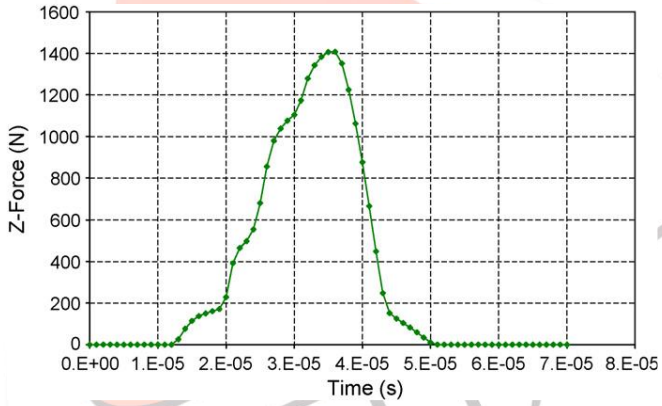

Fig. 4. The *z*-force (i.e. the resistance force) on the impacting ball during the impact event for Case I in Table 2.

A detailed examination of Fig. 4 also reveals that the contact time for a WC ball of 5 m/s impacting the C-2000 plate is in the order of 4×10^{-5} s. In the first 2.5×10^{-5} s, the *z*-contact force continues to increase, while in the last 1.5×10^{-5} s the *z*-contact force exhibits a steady decrease. This entire contact process with a variation in the *z*-contact force can be understood in terms of the transformation from the kinetic energy of the ball to the deformation energy of the work-piece, which results in deceleration of the ball during the impact process and eventually detachment of the ball from the work-piece. The residual *x*- and *z*-stresses after detachment of the ball can be found in Fig. 3(a and b) after 5×10^{-5} s. Thus, it can be concluded from Fig. 3 that the residual *x*-stress (i.e., the stress in the plane of the plate) is compressive in nature, whereas the residual *z*-stress (i.e., the stress in the direction of the plate thickness) is in tension.

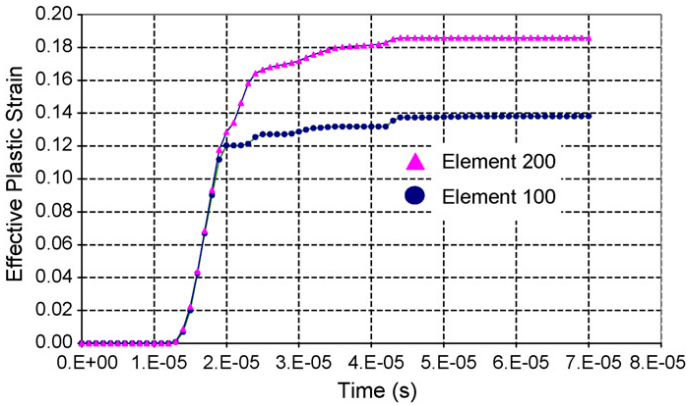

Fig. 5. The effective plastic strain in the work-piece right at and slightly beneath the contact point with the impacting ball (i.e., elements 100 and 200 in Fig. 1b, respectively) as a function of the impacting time for Case I in Table 2.

Fig. 5 shows the effective plastic strain in the work-piece right at and below the contact point with the ball as a function of the impacting time. It is noted that the effective plastic strain in the work-piece at the contact point with the ball is lower than that at the location below the contact point. This result is consistent with the Hertz theory of elastic contact, which predicts that the maximum shear stress and thus the effective plastic strain within the deformed work-piece are not at the contact point, but slightly below the contact point.

The residual in-plane compressive stress profile in the SNH-processed of C-2000 plate is relatively more complicated than that in most of the SP-processed componenets. In spite of this complication, the residual compressive stress profile is still consistent with the previous SP analysis, which shows that the maximum in-plane compressive stress can appear at the very surface if the work-piece has a very high work-hardening capacity. Therefore, it is complicated in-plane residual stress profile in the SNH-processed C-2000 alloy, i.e., a decrease in the compressive stress first as the position moves away from the impacted surface, which is followed by an increase and then further decrease until the change of sign, can be understood by overlapping of the typical residual compressive stress profile (that is, an increase in compressive stresses followed by a decrease until the change of sign) with the profile resulting from the work-piece with high work-hardening capacities as in the case of the C-2000 alloy.

The residual *z*-displacement profile in the work-piece after the single impact is shown in Fig. 8. The distance between the maximum and minimum points is ~70 μm which gives rise to the peak–valley (PV) value. A previously related study has shown that the PV value is a good indicator of the surface roughness, that is, the higher the PV value, more rough is the surface [8]. It is noted that a WC ball of 7.8 mm in diameter has generated a PV value of ~70 μm. Therefore, this analysis indicates that the PV value is about 1% of the ball diameter.

2.2. SNH process with Multiple impacts

Single impact events modeling and analysis can provide invaluable insights into the physical process during impact. Also many results from the single impact analysis can be utilized to predict the properties and behaviors of the work-piece after multiple impacts. For example, it has been shown that the residual stress profile derived from the simulation of single impact is very similar to the experimental analysis from multiple impacts. Also multiple impacts simulation could offer direct comparisons with the results from the single impact modeling.

2.3. SP process with Single impacts

Fig. 6 shows the effective plastic strain as a function of the location measured from the surface impacted for a typical SP process (i.e., Case II in Table 2). It can be seen that the depth of the plastic zone obtained from the SP process (~200 μm) is substantially smaller than that (~1200 μm) achieved from the SNH process .

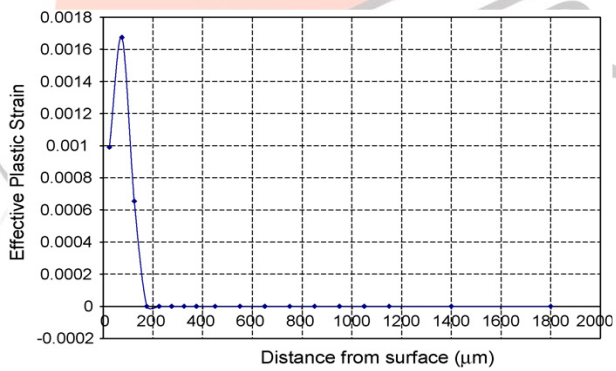

Fig. 6. The effective plastic strain profile within the work-piece measured from the contact point after the single impact for Case II in Table 2.

Furthermore, the magnitude of the maximum effective plastic strain has been reduced from 0.187 for the SNH process to 0.0016 for the SP process. Three major conclusion can be drawn from these results. First, the depth of the work-hardened layer is much less for the SP-processed work piece than that for the SNH-processed work-piece. Second, the thickness of the surface layer with residual compressive stresses is expected to be much less for the SP-processed work-piece. Finally, the effective plastic strain of the SNH-processed work-piece is about 100 times that of the SP-processed work-piece. Since large plastic strain is necessary for the formation of nano-grains [9,10], the SNH process is thus more effective in inducing surface nanostructuring. Furthermore, the thickness of the nanostructured surface layer in the SNH-processed work-piece will be much larger than that in the SP-processed counterpart, if the effective plastic strain generated in the SP process exceeds the critical plastic strain for the formation of nano-grains. This explains why few cases are reported for the formation of a nanostructured surface layer in the SP-processed work-piece.

Fig. 7 also reveals an additional piece of information, showing that the maximum residual compressive stress in the SP-processed work-piece is about 10 times lower than that in the SNH-processed work-piece. Thus, the SNH-processed work-piece has a thicker surface layer containing larger values of residual compressive stresses than the SP-processed work-piece The analysis above clearly indicates that the SNH-processed work-piece has a thicker work-hardened layer, a deeper surface region with larger residual compressive stresses, and the presence of a nanocrystalline surface layer. All these three factors are beneficial to the fatigue resistance. Therefore, it is expected that the SNH-processed work-piece could have a better fatigue resistance than the SP-processed counterpart. Although such an expectation remains to be confirmed experimentally, a recent work has shown that fatigue strength can be improved by the SNH process by 50% for the C-2000 alloy [15].

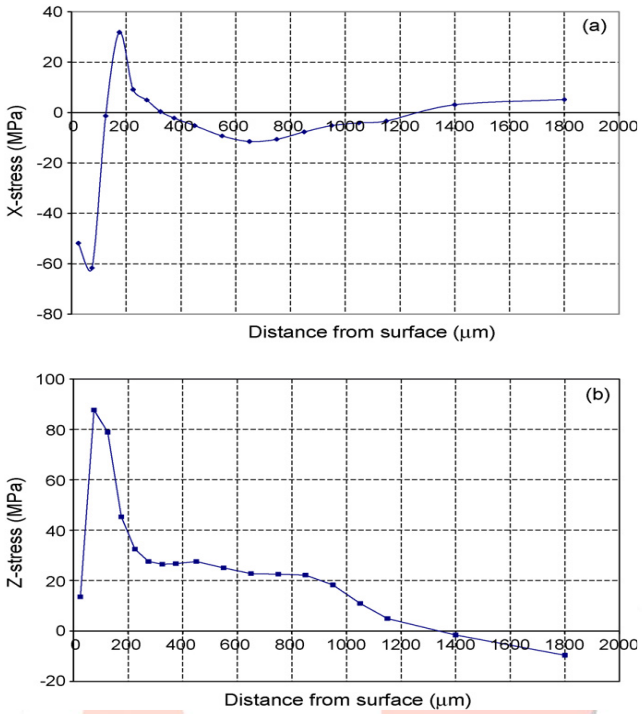

Fig. 7. (a) The residual x-stress and (b) z-stress profiles within the work-piece measured from the contact point after the single impact for Case II in Table 2.

3.4. Hypothetical high-speed SP process with Single impacts

Observation obtained by finite element simulation of the hypothetical high-speed SP process (i.e., Case III in Table 2) are shown in Table 3. For comparison, the major parameters obtained from Cases I and II are also included in Table 3. A comparison between the conventional SP and hypothetical SP reveals that for a given shot size, the maximum effective plastic strain increases with the kinetic energy of shots. As expected, the depth

Table 3

Case ID	Ball diameter (mm)	Impact velocity (m/s)	Kinetic energy (J)	Depth of plastic zone (mm)	Maximum effective plastic strain	Maximum compressive stress (MPa)
SNH	7.86	5	0.0476	~1.5	0.18	-650
SP	0.3	50	0.000265	~0.19	0.0016	-63
High-speed SP	0.3	670	0.0476	~1.1	0.315	-500

of the plastic zone increases with the kinetic energy of balls for a given ball size. When the kinetic energy is kept constant (Case I versus Case III in Table 3), smaller shots generate a larger effective plastic strain than larger balls. However, larger balls lead to a larger depth of the plastic zone. Thus, the finite element analysis suggests that for a given kinetic energy, smaller balls are quicker in creating a nanocrystalline surface layer than larger balls, whereas larger balls are more effective in creating a thicker nanocrystalline surface layer than smaller balls.

III. CONCLUSION

Difference between shot peening, nanostructuring and hardening processes have been analysed by using finite element modeling technique. The results indicate that the SNH process, which shows repeated impingments of the work-piece surface with large balls, has a higher kinetic energy, produces a thicker hardened layer and surface region with larger residual compressive stresses, and generates higher effective plastic strains than the shotpeened process. As a result of higher effective plastic strains, SNH can produce nanograins more effectively then SP process. Furthermore, if a nanograined surface layer is formed via SP, the thickness of this nanocrystalline surface layer will be much thinner than that produced via SNH. When the kinetic energy is fixed, smaller

balls are quicker in creating a nanocrystalline surface layer than larger balls, whereas larger balls are more effective in creating a thicker nanocrystalline surface layer than smaller balls. Since the SNH-processed work-piece has a thicker work-hardened layer and a deeper surface region with larger residual compressive stresses with the presence of a nanocrystalline surface layer, it is expected that SNH has the potential to improve the fatigue resistance more than SP does.

REFERENCES

[1] N.R. Tao, Z.B. Wang, W.P. Tong, M.L. Sui, J. Lu, K. Lu, Acta Mater. 50 (2002) 4603–4616.
[2] K.Y. Zhu, A. Vassel, F. Brisset, K. Lu, J. Lu, Acta Mater. 52 (2004) 4101–4110.
[3] N.R. Tao, M.L. Sui, J. Lu, K. Lu, Nanostruct. Mater. 11(1999) 433–440.
[4] X. Wu, N. Tao, Y. Hong, B. Xu, J. Lu, K. Lu, Acta Mater. 50 (2002) 2075–2084.
[5] C.H. Chen, R.M. Ren, X.J. Zhao, Y.J. Zhang, Trans. Nonferrous Met. Soc. China 14(2004) 215–218.
[6] G. Ma, Y. Luo, C.H. Chen, R.M. Ren, W. Wu, Z.Q. Li, Y.S. Zeng, Trans. Nonferrous Met. Soc. China 14(2004) 204–209.
[7] K. Dai, J. Villegas, L. Shaw, Scr. Mater. 52 (2004) 259–263.
[8] K. Dai, J. Villegas, Z. Stone, L. Shaw, Acta Mater. 52 (2004) 5771– 5782.
[9] M. Umemoto, K. Todaka, K. Tsuchiya, Mater. Sci. Eng. A375–377 (2004) 899–904.
[10] K. Todaka, M. Umemoto, Y. Watanabe, K. Tsuchiya, Mater. Sci. Forum 449–452 (2004) 1149–1152.
[11] J. Villegas, Investigation of the effects of the surface nanocrystallization and hardening (SNH) process on bulk metallic components, Ph.D. Thesis, University of Connecticut, 2005.
[12] G. Liu, S.C. Wang, X.F. Lou, J. Lu, K. Lu, Scr. Mater. 44 (2001)1791– 1795.
[13] J. Villegas, K. Dai, L. Shaw, P. Liaw, in: L. Shaw, C. Suryanarayana, R. Mishra (Eds.), Processing and Properties of Structural Nanomaterials, TMS, Warrendale, PA, 2003, pp. 61–68.
[14] Z.B. Wang, N.R. Tao, S. Li, W. Wang, G. Liu, J. Luc, K. Lu, Mater. Sci. Eng. A352 (2003) 144–149.
[15] J. Villegas, L. Shaw, K. Dai, W. Yuan, J.W. Jian, P. Liaw, D.L. Klarstrom, Philos. Mag. Lett. 85 (2005)427.
[16] Y.F. Al-Obaid, Mech. Mater. 19 (1995) 251–260.
[17] K. Schiffner, C. Droste gen. Helling, Computers and Structures 72 (1999) 329–340.
[18] J.O. Hallquist, LS-DYNA Theoretical Menu, Livermore Software Technology Corporation, 1998.